# Spin fluctuations in the antiferromagnetic metal Nb$_{12}$O$_{29}$

J.-G. Cheng,[1] J.-S. Zhou,[1,*] J. B. Goodenough,[1] H. D. Zhou,[2] C. R. Wiebe,[2] T. Takami,[3] and T. Fujii[4]

[1]*Texas Materials Institute, University of Texas at Austin, Austin, Texas 78712, USA*
[2]*NHMFL, Florida State University, Tallahassee, Florida 32306, USA*
[3]*Department of Physics, Nagoya University, Furo-cho, Chikusa, Nagoya 464-8602, Japan*
[4]*Cryogenic Research Center, University of Tokyo, Bunkyo-ku, Tokyo 113-0032, Japan*

We report a comprehensive study of the monoclinic Nb$_{12}$O$_{29}$ that includes material synthesis, chemical and structural characterization, and measurements of physical properties as a function of temperature, magnetic field, and high pressure. The high-pressure structural study has been carried out up to 71 kbar. Critical behavior analysis of $\rho(T)$ and $C_p(T)$ as $T_N$ is approached from $T_N^+$ is consistent with the picture of localized spins in this metallic antiferromagnet. These results also indicate that thermally driven critical fluctuations are confined to a temperature range in the vicinity of $T_N \approx 12$ K. The thermoelectric power, however, is strongly enhanced at $T < 70$ K. The peculiar temperature dependence of the thermoelectric-power enhancement at low temperatures is consistent with predictions based on quantum critical fluctuations. We have also shown that the enhancement is suppressed under either a magnetic field or hydrostatic pressure.

## I. INTRODUCTION

Magnetic and transport properties of Nb$_{12}$O$_{29}$ were first reported by Cava *et al.*[1,2] with a motivation to compare this antiferromagnetic, quasi-one-dimensional (1D), $d^1$ system with the copper oxides in which high-$T_c$ superconductivity can be obtained by doping an antiferromagnetic, quasi-two-dimensional (2D), $d^9$ Mott insulator. Nb$_{12}$O$_{29}$ is a rare example of long-range magnetic order in niobium oxides.[2] The metallic conductivity down to 2 K and antiferromagnetic ordering mean that either electrons in the conduction band interact with localized spins or the electrons at the Fermi surface are unstable against the magnetic state similar to the magnetism proposed by Stoner.[3] In the localized-charge picture, the formula Nb$_{12}$O$_{29}$ can be written as Nb$_2^{4+}$ Nb$_{10}^{5+}$O$_{29}$, where the electrons from the two Nb$^{4+}(4d^1)$ per block of 12 NbO$_{6/2}$ octahedra are responsible for the electrical and magnetic properties. Based on the high-temperature Curie-Weiss (C-W) behavior, a model where one electron per formula unit is localized at, perhaps, a specific site of Nb$^{4+}$ and the other electron is delocalized has been proposed to account for the coexistence of metallic conductivity and antiferromagnetic ordering at $T_N = 12$ K.[1,2] Although this early study has triggered several follow-up investigations on a series of compounds of niobium oxide, the microscopic picture of the electronic state falls far short of being well understood. A Curie-Weiss fitting of $\chi$ versus $T$ of the paramagnetic phase cannot be taken as conclusive evidence of localized spins since an itinerant-electron magnetic system can also exhibit a Curie-Weiss behavior where the Curie constant is no longer related to a $\mu_{eff}$ of a localized moment.[4] However, a $\mu$SR study has provided stronger evidence for the presence of localized spins.[5] A reported broader transition at $T_N$ signals a low-dimensional exchange pathway, which should enhance critical fluctuations in the vicinity of $T_N$ or even over a broader temperature range. How thermally driven critical fluctuations and possible spin fluctuations in-fluence transport properties of the compound remains unknown.

Nb$_{12}$O$_{29}$ has two crystal structures: a monoclinic (M) phase and an orthorhombic (O) phase.[6] Both the monoclinic and orthorhombic polymorphs of Nb$_{12}$O$_{29}$ have a basic unit, a block of $4 \times 3$ corner-shared NbO$_6$ octahedra. These blocks are connected along the $a$ axis by an interface of edge-shared NbO$_6$ octahedra with a second block that slides by 1.5 octahedra along the $c$ axis from the first block. As shown in Fig. 1, the structural difference between the orthorhombic and monoclinic phases is that the unit cell includes one sliding block in the orthorhombic phase, two sliding blocks in the monoclinic phase. Zigzag chains in a layer have edge-shared interfaces with others in the layer below by sliding 0.5 octahedron along the $b$ axis. Octahedra in a block are highly distorted and not uniform. A neutron-diffraction study[7] showed only one octahedron in which the Nb-O bond-length variation is relatively small at 2 K; it is in a specific location in the center of a block of the M Nb$_{12}$O$_{29}$. The authors of this study have assumed that the specific octahedron is occupied by Nb$^{4+}$:$d^1$ since an octahedron with a Nb$^{5+}$:$d^0$ ion commonly shows a ferroelectric displacement like the Ti$^{4+}$:$d^0$ in BaTiO$_3$. A calculation based on the valence sum rule in the same neutron study, however, indicated that the site having the smallest bond-length variation has its valence close to 5. As for the orthorhombic phase of Nb$_{12}$O$_{29}$, its physical properties reported in the literature are controversial. The early study[1] showed that the orthorhombic phase is metallic and antiferromagnetic below $T_N \approx 12$ K. However, a recent study by Andersen *et al.*[6] claimed that the magnetic phase can only be found in the M phase although both the M and the O phases show a Curie-Weiss behavior of their paramagnetic susceptibility. Single-crystal x-ray diffraction (XRD) (Ref. 8) at 200 K showed that the bond-length variation in all octahedra in a block is too large for a localized spin Nd$^{4+}$ in the O phase. How the compound responds to hydrostatic pressure may give an important clue to
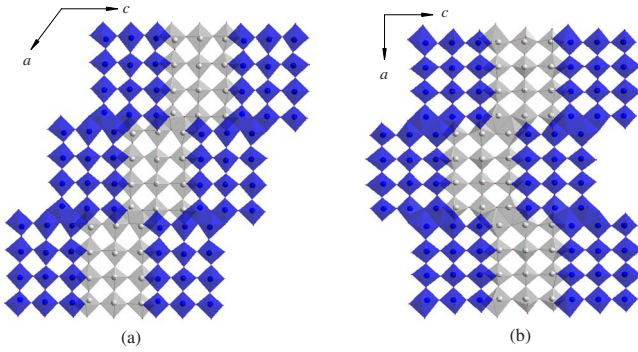
FIG. 1. (Color online) Crystal structures of $Nb_{12}O_{29}$, (a) monoclinic phase and (b) orthorhombic phase.

the electronic state. Although a recent high-pressure study[9,10] did not track down the pressure dependence of $T_N$ in their orthorhombic $Nb_{12}O_{29}$ sample, it showed a progressive transition from a metallic phase to an insulator phase below room temperature as pressure increases. This behavior under high pressure is just opposite to what we normally see in other materials. The authors proposed two possible solutions to their results: (1) a pressure-enhanced electron-electron correlation or electron-phonon interaction and (2) a pressure-induced amorphization. No justification for these two solutions was given in that report. A badly needed experiment is a structural study under high pressure that will tell directly whether the compound undergoes amorphization or a transition to some other phase. Nevertheless, this high-pressure study points out that the apparent antiferromagnetic metallic phase of the orthorhombic $Nb_{12}O_{29}$ is located at the boundary to a Curie-Weiss insulator phase without magnetic order, perhaps the same nonmagnetic phase reported by Andersen *et al.*[6] As far as we know, there is no high-pressure study on the M phase. A systematic study is clearly needed in order to address these issues, which motivated us to carry out material synthesis and characterization, measurements of thermodynamic and transport properties under high magnetic field and under high pressure, as well as a structural study under high pressure.

## II. EXPERIMENTAL DETAILS

Both monoclinic and orthorhombic $Nb_{12}O_{29}$ samples in this study were made from stoichiometric amounts of H-$Nb_2O_5$ and Nb metal. H-$Nb_2O_5$ was first obtained by firing the commercially available $Nb_2O_5$ for 24 h at 1100 °C.[11] The mixture of H-$Nb_2O_5$ and Nb was thoroughly ground and then cold pressed into pellets ($\sim$3 mm in diameter). For cold pressing, powder was first filled into the center hole of a hard cardboard gasket; then the gasket with the sample powder was placed between two carbide anvils (15 mm in diameter) before applying a 20 T loading force. These pellets were wrapped in molybdenum foil and heated in a vacuum furnace at pressures below $10^{-6}$ Torr. M $Nb_{12}O_{29}$ can be obtained by heating at 1150 °C for 24 h; this phase is stable during the subsequent treatment at 1200 °C for 5, 12, 24, and 60 h. The orthorhombic $Nb_{12}O_{29}$ (O_vac) was obtained by heating 24 h at 1400 °C. High-density pellets obtained by

cold pressing were found to be critical to obtain single-phase samples in our study. Pellets with lower density made under a loading force of $\sim$5 tons with a 10 mm diameter die always contained an unreacted $Nb_2O_5$ impurity. Furthermore, cold pressing also helps to minimize the grain-boundary effect on the electrical properties. Our high-density pellets show the lowest resistivity reported for $Nb_{12}O_{29}$ in the literature. Phase purity was examined with powder XRD on a Philips X'pert diffractometer with Cu anode. The Nb:O ratio was determined from thermogravimetric analysis (TGA) with a Perkin-Elmer Series 7 Thermal Analyzer in air at 800 °C. We have also found that a high-pressure O (O_hp) phase may be obtained by treating the M phase sample under 6 GPa at ambient temperature. However, XRD peaks are broader than that of the samples sintered in a vacuum furnace. dc magnetic susceptibility was measured with a superconducting quantum interference device (SQUID) magnetometer (Quantum Design). A four-probe method was used to measure the resistivity. The specific-heat measurement was performed on a physical properties measurement system (Quantum Design) with the two-$\tau$ relaxation method. Measurements of thermoelectric power, including that under hydrostatic pressure, were taken with a homemade apparatus. In the pressure measurement, Daphne 7373 oil was used as the pressure medium and a manganin-wire coil served as both the heater and pressure manometer. The structural study under high pressure was carried out with a diamond-anvil cell (DAC) mounted on a four-circle diffractometer (Bruker P4) with Mo anode. A small amount of $CaF_2$ powder was mixed with the sample to show the pressure inside the chamber filled with a mixture of methanol and ethanol as the pressure medium. Diffraction from the sample inside the DAC was collected with an image plate from Fujifilm. We have used the software FIT2D to integrate the diffraction pattern into intensity versus $2\theta$.

## III. RESULTS AND DISCUSSION

### A. Material characterization

Figure 2 shows the XRD of several samples sintered at different temperatures and different duration times. The major features of the XRD profile look similar between these two phases. The small structural difference between the M and O phases is reflected in the XRD for the $d$ spacing of 3–4 Å. While both end members in these samples, i.e., one fired at 1150 °C for 24 h and the other at 1400 °C for 24 h, match perfectly the monoclinic phase and the orthorhombic phase in the literature, respectively, the samples fired at intermediate temperatures and different duration times show how the orthorhombic phase evolves from the monoclinic phase. The M phase is stable over a relatively narrow range of temperature. The O phase appears at a sintering temperature around 1250 °C. From these XRD results, the orthorhombic phase is distinguished by (1) a clear separation between the (011) and (111) peaks, (2) the (106) peaks appear as a clear shoulder near (006), and (3) the (800) peak, one of the three major peaks, has an intensity almost triple that of the (011) and (006). These characteristics are useful in identifying whether pressure can induce a phase transition as is
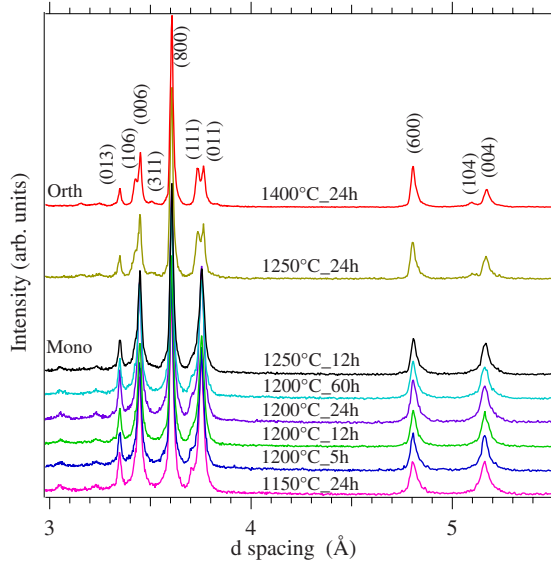
FIG. 2. (Color online) X-ray ($\lambda = 1.54187$ Å) powder diffraction of $Nb_{12}O_{29}$ obtained by annealing at different temperatures and duration times. All peaks can be fully indexed in the monoclinic phase with $A2/m$ space group and $a = 15.63(1)$ Å, $b = 3.832(3)$ Å, $c = 20.70(6)$ Å, and $\beta = 112.7°$; in the orthorhombic phase with $Amma$ space group and $a = 28.830(4)$ Å, $b = 3.8267(6)$ Å, and $c = 20.685(3)$ Å.

discussed below. Both the M phase and the O phase can be easily oxidized to $Nb_2O_5$ in air and the weight change as monitored by TGA has been used to calculate the Nb:O ratio of the testing sample to be 1:2.41(1), which agrees within instrumental resolution with the expected: 1:2.417. Although the XRD shows that single M and O_vac phases can be achieved by using the synthesis method described, the transport and magnetic measurements indicate that there is some minority M phase in our O_vac samples.

The dc magnetic susceptibilities $\chi(T)$ shown in Fig. 3(a) were measured on heating from 5 to 300 K under $H = 1$ T after zero-field cooling. The M phase and the O_vac phase in our study exhibit nearly identical magnetic susceptibilities. The $\chi^{-1}(T)$ curves show a C-W behavior for both polymorphs over a wide temperature range 30–300 K. Fitting to the C-W law,

$$\chi - \chi_0 = C/(T + \theta_{CW}), \quad (1)$$

where $\chi_0 \sim 1 \times 10^{-5}$ emu/mol $NbO_{2.417}$ is a temperature-independent contribution, yields a Curie constant $C = 2.83 \times 10^{-2}$ emu K/mol $NbO_{2.417}$ and a Weiss temperature $\theta_{CW} = -28.8$ K for the monoclinic phase and $C = 2.75 \times 10^{-2}$ emu K/mol $NbO_{2.417}$ and $\theta_{CW} = -22.9$ K for the orthorhombic phase, respectively. The calculated effective moments show that only $\sim 45\%$ of the $4d$ electrons contribute to the localized moment if we assume simply $S = 1/2$ and $g = 2$. These values for the M phase sample are in good accord with previous reports.[1,2,5,6] Since the O phase has been reported to be paramagnetic to the lowest temperature, our O_vac phase sample appears to include some M phase. The O_hp phase is paramagnetic to 5 K.
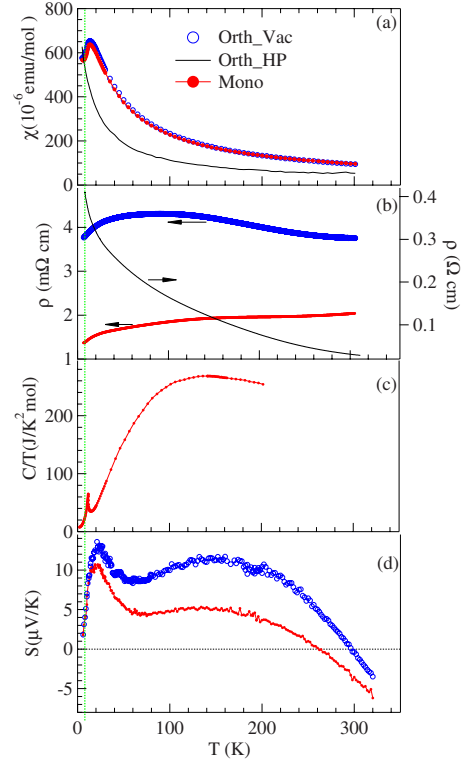


FIG. 3. (Color online) Temperature dependences of (a) magnetic susceptibility with $H = 1$ T, (b) resistivity, (c) specific heat (the monoclinic phase only), and (d) thermoelectric power in the monoclinic phase and the orthorhombic phase of $Nb_{12}O_{29}$.

As shown in Fig. 3(b), the temperature dependence of resistivity $\rho(T)$ of the M phase is similar to that previously reported. Although the M phase and the O_vac phase cannot be distinguished from $\chi(T)$, the $\rho(T)$ of the O_vac phase is higher than that of the M phase and shows a semiconductor thermal behavior at $T > 100$ K. In contrast, the O_hp phase shows a much higher resistivity.

The specific heat $C_p(T)$ and thermoelectric power $S(T)$ in Figs. 3(c) and 3(d) have not been reported before on this compound. A $\lambda$-shaped peak in $C_p$ near $T_N$ is typical for a magnetic transition. Although $S(T)$ for the M and O_vac phases are slightly different from each other, neither behaves like the Mott diffusive $S(T)$ found in a regular metal. A pronounced enhancement of $S(T)$ sets in well above $T_N$. As demonstrated and discussed below, the magnetic field dependence and pressure dependence of $S(T)$ help to identify the origin of this low-temperature enhancement.

### B. Spin fluctuations and the critical behavior near $T_N$

Since results of the M phase $Nb_{12}O_{29}$ are consistent with that in the literature, we have concentrated on the M phase for studying the critical behavior. Fisher and Langer[12] have shown that $d\rho/dT$ should have a temperature dependence similar to that of $C_m(T)$ in the vicinity of a magnetic transition temperature for magnetic metals. We apply the same analysis as for the critical behavior of ferromagnetic metals[13–15] to the M phase $Nb_{12}O_{29}$. Figures 4(a) and 4(b) show the zoom-in plots of the temperature dependences of
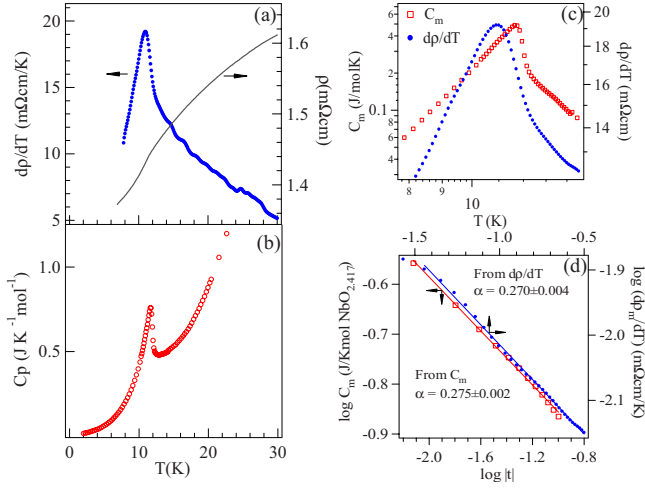
FIG. 4. (Color online) Temperature dependences of (a) $d\rho/dT$ and resistivity $\rho$ and (b) specific heat $C_p$ in a narrow temperature range near $T_N$ in the monoclinic phase $Nb_{12}O_{29}$. (c) A log-log plot of temperature dependences of $d\rho/dT$ and $C_m$ near $T_N$. (d) The same plot of (c) at $T > T_N$.

resistivity, the derivative $d\rho/dT$ and $C_p$ in the vicinity of $T_N$. The spin contribution $C_m$ can be obtained by subtracting the lattice contribution in $C_p$ and its temperature dependence has been plotted in Fig. 4(c) together with $d\rho/dT$. Whereas the essential feature of the critical fluctuations in the $C_m$ and $d\rho/dT$ data is nearly identical on both sides of a spin ordering temperature for ferromagnetic metals, we found it to be present only at $T > T_N$ for the antiferromagnetic metal $Nb_{12}O_{29}$. The same situation also occurs in the metallic antiferromagnet $PbCrO_2$.[16] The critical behavior of $C_m$ can be described[17] by

$$C_m^+ \sim (A^+/\alpha)|t|^{-\alpha}, \quad T > T_N, \qquad (2)$$

where $t = (T - T_N)/T_N$ and $\alpha$ is the critical exponent. The log-log plot at $T > T_N$ of Fig. 4(d) indeed shows good linearity for both $d\rho/dT$ and $C_m$, and linear fittings give $\alpha = 0.270 \pm 0.004$ and $0.275 \pm 0.002$. The similarity of the critical exponents does not help to distinguish whether spins are localized or itinerant since it has been found in metals with localized spin as well as in well-known itinerant-electron ferromagnetic metals such as $ZrZn_2$.[18] The magnitude of $\Delta C_m$ at $T_c$ or $T_N$, however, reveals the most important information about the spin state. In band-electron magnetism, only a very small portion of the electronic states near the Fermi energy is magnetized. Therefore, $\Delta C_m$ is normally very small; it is about 0.15 mJ K$^{-1}$ mol$^{-1}$ in $ZrZn_2$. In contrast, it is as large as 4 J K$^{-1}$ mol$^{-1}$ in the $Nb_{12}O_{29}$, which is comparable to a $\Delta C_m \sim 20$ J K$^{-1}$ mol$^{-1}$ in $LaMnO_3$, a typical localized-electron antiferromagnet. This observation is consistent with the conclusion of a $\mu$SR study on the same compound. The singularity of $d\rho/dT$ above $T_N$ arises mainly from the scattering of conduction electrons from short-range spin fluctuations above the long-range magnetic ordering temperature.[12] Now we focus on whether thermally driven critical fluctuations are sufficient to account for the peculiar temperature dependence of $S(T)$ at $T > T_N$.
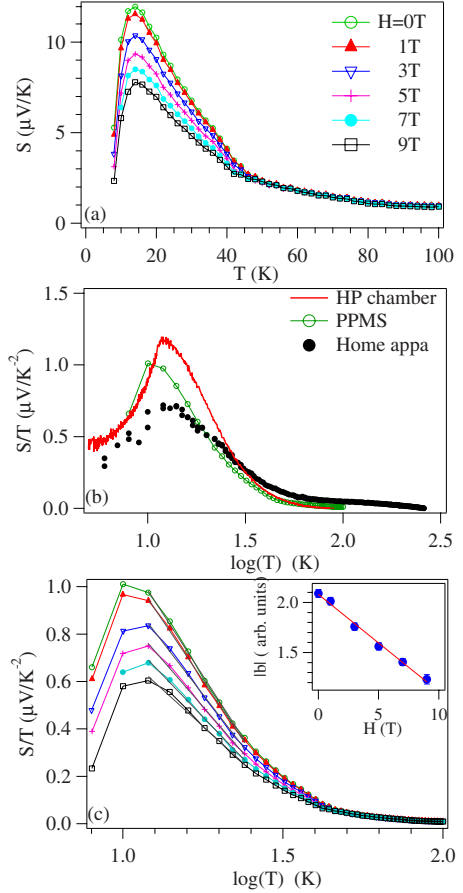


FIG. 5. (Color online) (a) Temperature dependences of thermoelectric power of the $Nb_{12}O_{29}$ under different magnetic fields; (b) The $S/T$ versus log $T$ plot of $S(T)$ data collected with three different instruments; (c) The $S/T$ versus log $T$ plot of $S(T)$ under different magnetic field in (a). Inset: the absolute value of $b$ versus magnetic field $H$ ($b$ is the slope of a linear fitting in $S/T$ versus log $T$ plot within the temperature range 12–25 K).

The enhancement of thermoelectric power around $T_N$ in Fig. 3(d) could be attributed to (1) the phonon-drag effect normally found at low temperatures in metals in which the electron-phonon interaction is weak, (2) thermally driven critical fluctuations, and (3) quantum critical fluctuations that take place where a long-range magnetic transition temperature is suppressed to zero. In the case of quantum critical fluctuations, the influence can be seen at finite temperatures near a quantum critical point approached from the magnetic phase or the nonmagnetic phase.[19] The phonon-drag effect can be easily ruled out by the fact that the enhancement of $S(T)$ is dramatically reduced by applying a magnetic field in Fig. 5(a). The anomaly of $S(T)$ due to thermally driven critical fluctuations in magnetic metals is normally small and does not extend to temperatures much higher than $T_c$ or $T_N$.[20] The ruling-out procedure does not mean the quantum critical fluctuations are the only source for an enhanced thermoelectric power at low temperature. A theoretical model[21] has predicted a linear relationship of $S/T$ versus log $T$ if quantum fluctuations play a role to enhance the thermoelectric power at low temperatures. In order to test this possibility, we have plotted the $S(T)$ obtained from three different apparatuses as
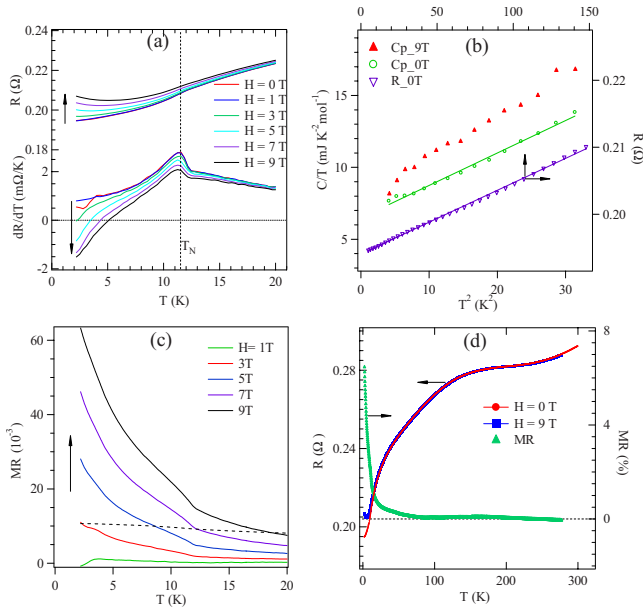
FIG. 6. (Color online) (a) Temperature dependences of resistance $R$ and $dR/dT$ under different magnetic fields; (b) plots of specific heat $C_p/T$ versus $T^2$ and resistance $R$ versus $T^2$; (c) temperature dependence of the magnetoresistance coefficient MR under different magnetic fields in the temperature range near $T_N$; dashed line is the prediction from the Lorentz force of Eq. (5) in the text for $H=9$ T; (d) temperature dependence of resistance $R$ under 0 and 9 T and the MR coefficient between them over a broad temperature range from 2 to 300 K. Arrows in (a) and (c) point to the direction of increasing magnetic field.

$S/T$ versus log $T$. Due to instrumental factors, the peak magnitude and the on-set temperature of the enhancement differ. However, over a broad temperature range at $T>T_N$, curves can be fit linearly and the slope is highly sensitive to a magnetic field as shown in the inset of Fig. 5(c). Although a formula showing the relationship between the enhancement of $S$ and magnetic field is not available, the magnetic field dependence of $S$ is qualitatively compatible with a model of quantum critical fluctuations.[22]

### C. Magnetoresistance

Figure 6(a) shows the temperature dependence of resistance in different magnetic fields. At $H=0$ T, the M phase of $Nb_{12}O_{29}$ is metallic down to 2 K; $R(T)$ can be fit well with the power law $R\sim T^2$ within 2–12 K, characteristic of a Fermi liquid. Provided that the contribution from spin-wave excitations is weak, the specific heat $C_p$ at low temperature in Fig. 6(b) can be fit with $C_p=\gamma T+\beta T^3$ with the fitting parameter $\gamma=6.14$ mJ mol$^{-1}$ K$^{-2}$. This $\gamma$ value and the power-law fitting of $R(T)$ at low temperatures indicate that $Nb_{12}O_{29}$ is a regular metal. $T_N$ as monitored by an anomaly in the curve $dR/dT$ versus $T$ in Fig. 6(a) does not show any noticeable change with magnetic field. The magnetoresistance (MR) effect is defined as

$$\Delta R/R(0,T) = [R(H,T) - R(0,T)]/R(0,T). \quad (3)$$

Like a regular metal, $Nb_{12}O_{29}$ exhibits the positive MR shown in Fig. 6(c), which increases as temperature de-

creases. However, the maximum MR effect from the Lorentz force, which is described by[23]

$$\Delta R/R(0,T) = H^2/[aR(0,T)^2 + bH^2] \quad (4)$$

can only account for a very small fraction of the MR effect observed. On the other hand, all MR effects due to spin-wave excitations and spin fluctuations are generally negative and the maximum MR effect occurs at magnetic transition temperatures.[24,25] We have to look for an alternative reason for the positive MR effect found in the $Nb_{12}O_{29}$. Figure 6(d) shows that the positive MR effect under $H=9$ T takes place at $T\approx60$ K, nearly the same temperature where the enhancement of $S(T)$ sets in. The MR effect due to thermally driven spin fluctuations may be tracked down by a small hump of the curve of $\Delta R/R(0,T)$ versus $T$ at $T_N$; but we have observed a large positive MR effect spreading over a broad temperature range below 60 K. The resistance increase at $T<60$ K is likely due to a field-induced phase transition to a nonmagnetic insulator phase. As a matter of fact, a semiconductor behavior at $T<5$ K is clearly visible under $H>3$ T in Fig. 6(a). The two-phase scenario can be supported by a specific-heat measurement under a magnetic field. As shown in the plot of $C_p/T$ versus $T^2$ in Fig. 6(b), the curve for $H=9$ T is above that for $H=0$ T, which is just opposite to that observed in the single phase of a regular ferromagnet or antiferromagnet. The magnetic field clearly creates some new degree of freedom that, we believe, is due to fluctuations between two phases. A down turn as temperature approaches zero in the curve of $C_p/T$ versus $T^2$ under $H=9$ T in Fig. 6(b) points to a much reduced $\gamma$ under a magnetic field, which is consistent with a semiconductive behavior in $R$ versus $T$ under 9 T in Figs. 6(a) and 6(d).

### D. Thermoelectric power and crystal structure under high pressure

Figure 7(a) shows the temperature dependence of thermoelectric power under different pressures. At ambient pressure, the $S(T)$ obtained in the high-pressure chamber repeats the essential features that have been observed with other instruments shown in Fig. 5(b). Whereas the thermoelectric power at $T>70$ K becomes independent of magnetic field, $S(T)$ is highly sensitive to hydrostatic pressure, especially at low temperatures and near room temperature. The low-temperature enhancement of $S(T)$ that starts at about 70 K and peaks near $T=15$ K$>T_N$ is reduced under pressure and is nearly suppressed under $P=24$ kbar. This pressure-induced change, however, is reversible at least up to $P=24$ kbar. As seen from the inset in Fig. 7(b), a zoom-in plot of $S(T)$ in Fig. 7(a) at low temperatures and under ambient pressure, the long-range magnetic ordering at $T_N\approx11.5$ K changes the slope of $S(T)$ versus $T$. Therefore, thermally driven critical fluctuations appear not to influence the enhancement starting at 60 K. By tracking down the anomaly of $S(T)$ in Fig. 7(b) under different pressures, we are able to obtain the pressure dependence of $T_N$ in the M phase of $Nb_{12}O_{29}$. As shown in Fig. 7(b), $T_N$ is independent of pressure to within error bars. However, the anomaly of $S(T)$ at $T_N$ becomes smaller as pressure increases and disappears at
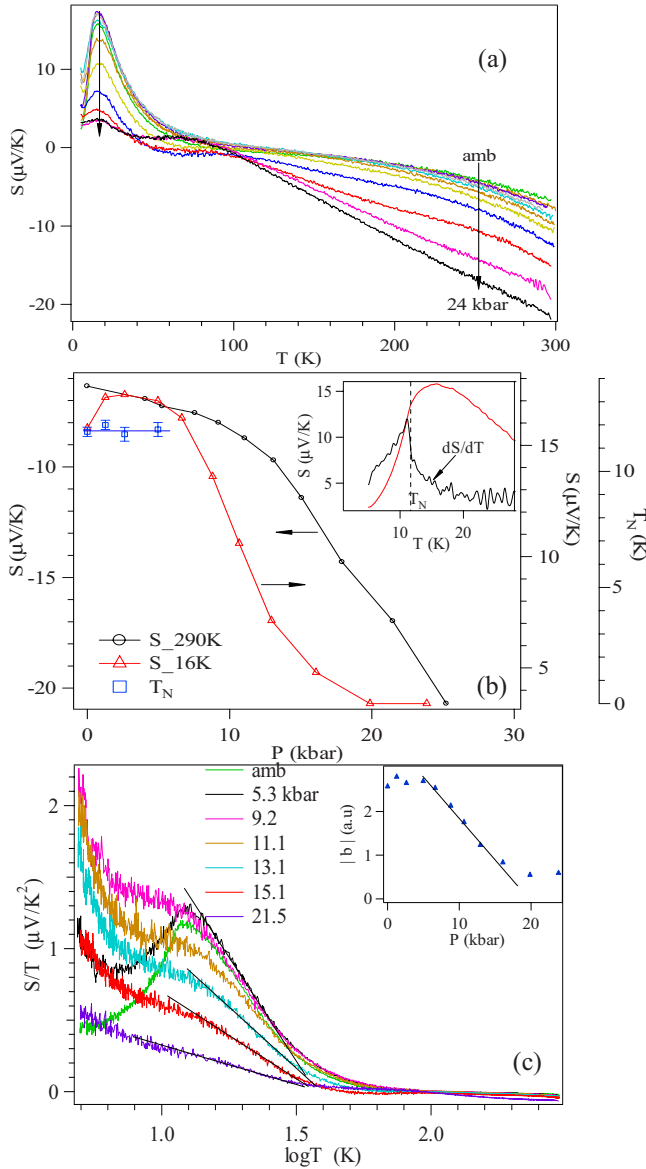
FIG. 7. (Color online) (a) Temperature dependence of thermoelectric power $S$ under different pressures; arrows inside the panel point to the direction of increasing pressure; (b) pressure dependence of Néel temperature $T_N$ and thermoelectric power at 16 and 290 K; the inset shows how we define $T_N$ from the thermoelectric power measurements; (c) the $S/T$ versus $\log T$ plot of $S(T)$ under different pressures; the inset shows the slope of the linear fitting on the curve of $S/T$ versus $\log T$ as a function of pressure.

$P > 6$ kbar, which suggests that the antiferromagnetic phase is unstable under pressure and gives way to a nonmagnetic phase through a first-order transition. The pressure-independent $T_N$ at $P < 6$ kbar already signals a two-phase coexistence. Suppression of the antiferromagnetic phase under pressure has also been confirmed by a magnetization measurement under pressure with a miniature Be-Cu cell fitted into a commercial SQUID magnetometer. The antiferromagnetic transition signal detected at ambient pressure loses its strength once pressure is applied. Whether pressure here induces a structural transition to the O phase or some other structure needs to be clarified by the high-pressure structure

study presented below. It is also interesting to note that at the same pressure where the antiferromagnetism disappears, the peak of $S$ at around 16 K in Fig. 7(b) decreases dramatically as pressure increases further. In order to verify any pressure-induced change in quantum critical fluctuations in $S(T)$, we have made the plot of $S/T$ versus $\log T$ under selected pressures in Fig. 7(c). The linear dependence of $S/T$ versus $\log T$ found in 16 K $< T <$ 50 K at ambient pressure remains viable to the highest pressure in this study. Within approximately the same temperature range where the curve of $S/T$ versus $\log T$ can be fit linearly, lines with different pressures overlap each other up to $P \approx 6$ kbar, the highest pressure in which $T_N$ can be detected. The slope of this linear range starts to decrease under $P > 6$ kbar. Surprisingly, the decrease in the slope as a function of pressure to a pressure where the enhancement has essentially vanished can be fit with a straight line, see the inset of Fig. 7(c). We have shown in Fig. 5(c) that the slope also decreases linearly with increasing magnetic field.

A quantum critical point in a system is normally reached at low temperatures as the long-range magnetic ordering is suppressed by hydrostatic pressure, magnetic field, and chemical substitution. Anomalous transport properties, i.e., non-Fermi-liquid behavior and largely enhanced thermoelectric power, are typical of a quantum critical phenomenon. What is unusual in the M phase of $Nb_{12}O_{29}$ is that $T_N$ does not change whereas the volume fraction of the antiferromagnetic phase reduces under either hydrostatic pressure or magnetic field. The thermoelectric power is dominated by the most conductive phase in the case of a coexistence of multiphases provided that the most conductive phase retains a percolation connection. Although the volume fraction of the metallic, antiferromagnetic M phase decreases, a percolation connection through the phase remains in place up to $P$ =6 kbar. Therefore, there is no obvious change in the enhancement of $S$ up to this pressure.

We turn to the high-pressure structural study of the M phase of $Nb_{12}O_{29}$ in order to understand the pressure effect on the thermoelectric power. Figure 8 shows XRD results under different pressures that are typical in the pressure range up to 71 kbar. First of all, the compound does not undergo any pressure-induced amorphization, as can be seen by checking the full width at half maximum of a diffraction peak, e.g., the (400) peak at $2\theta = 24.7°$, as a function of pressure. This observation rules out the possibility of pressure-induced amorphization. At $P > 60$ kbar, pressure induces two obvious changes in the XRD: (a) the degenerate (011) +(302) and (20−6)+(21−1) peaks shown by arrows in the figure become much broader relative to other peaks and (b) the relative ratio of three major peaks in $2\theta = 24 - 27°$ starts to change. As mentioned in the discussion of Fig. 1, these changes indicate the monoclinic to orthorhombic phase transition under pressure. This pressure-induced phase transition is supported by the observation that the high-pressure-treated M phase, i.e., the O_hp phase, is a paramagnetic insulator down to 5 K.

Lattice parameters obtained through a least-squares fit of XRD are shown in Fig. 9. The relation of volume versus pressure has been fit with the Birch-Murnaghan equation
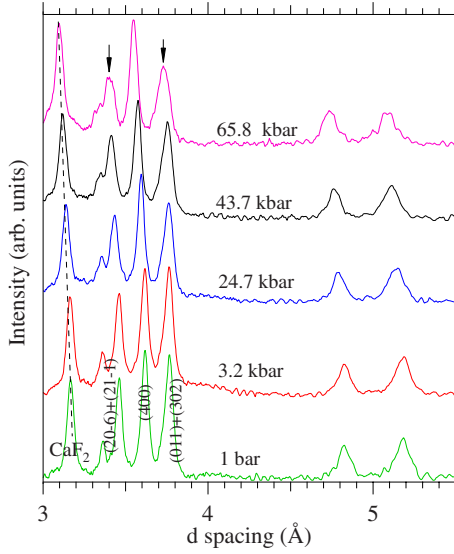
FIG. 8. (Color online) X-ray (Mo anode) powder diffraction of the M phase $Nb_{12}O_{29}$ under different pressures. Peak broadening for diffraction peaks indicated by arrows is due to the peak splitting associated with M/O phase transition.

$$P = \frac{3B_0}{2}\left[\left(\frac{V_0}{V}\right)^{7/3} - \left(\frac{V_0}{V}\right)^{5/3}\right]$$
$$\times \left\{1 + \frac{3}{4}(B'-4)\left[\left(\frac{V_0}{V}\right)^{2/3} - 1\right]\right\}. \qquad (5)$$

The bulk modulus $B_0 = 127$ GPa obtained from this fitting is a useful experimental value for calculation of the electronic structure of the M phase $Nb_{12}O_{29}$. As seen from the pressure dependence of lattice parameters in Fig. 9, $a$ and $c$ are much more compressible than $b$ whereas there is no noticeable change in angle $\beta$ under pressure in the M phase. A schematic drawing in Fig. 10 helps to envision the pressure effect on the electronic structure in the basic unit, a block of 4 $\times$ 3 corner-shared $NbO_6$ octahedra. Squeezing the block in the basal plane would force electrons that are 2D itinerant and primarily in a $zx$ orbital into orbitals of Nb-Nb bonds across a shared octahedral-site edge. As derived from the high-temperature magnetic susceptibility, the metallic conductivity and the critical behavior discussed above, one of two electrons in a block is likely localized on a $Nb^{4+}$ ion; the other spreads out in the 2D pathway formed within and between blocks. The magnetic coupling is due to the interaction between localized spins by way of the itinerant electrons through the Ruderman-Kittel-Kasuya-Yosida (RKKY) interaction as proposed in the $\mu$SR study.[5] Therefore, the pressure induced transfer of $zx$ itinerant electron into Nb-Nb bond states to make a metal-insulator transition would also suppress the antiferromagnetic phase but not the $\mu_{eff}$ of the localized spins. The $zx$ orbitals form an itinerant-electron band via 180° Nb-O-Nb interactions within a 4$\times$3 block and Nb-Nb bonds between blocks; this band does not overlap the $yz$ and $xy$ orbitals linking blocks along the $b$ axis across shared octahedral-site edges via Nb-Nb bonds, which gives the 2D character of the itinerant-electron state within an $a$-$c$
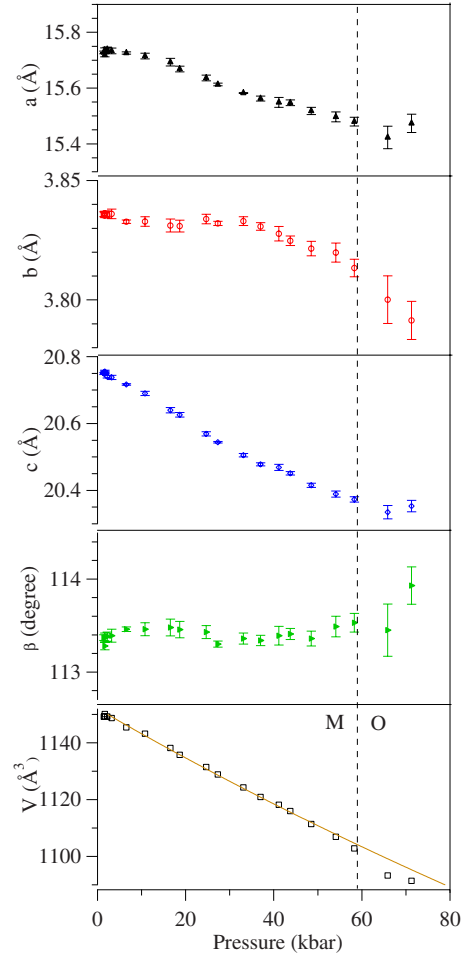


FIG. 9. (Color online) Pressure dependences of lattice parameters and the cell volume. At $P > 55$ kbar, the refinement with the monoclinic cell is poor and gives a larger error in the lattice parameters. The curve fitting in $V$ versus $P$ with the Birch-Murnaghan equation was made within $P < 55$ kbar; fitting parameters are $V_0 = 1152 \pm 0.33$, $B' = 4$ (fixed), and $B_0 = 127.5 \pm 1.6$.

plane. Raising the energy of the $zx$ band within a 4$\times$3 block relative to that of the orbitals of a Nb-Nb bond transfers electrons from the $zx$ band of a block to Nb-Nb bond states; such an electron transfer could account for the large compressibility of the 4$\times$3 blocks. Moreover, emptying of the $zx$ band within the blocks would suppress the indirect RKKY exchange interactions between the localized $Nb^{4+}:d^1$ configurations. The localized electrons have larger kinetic energy and therefore, by the virial theorem, a deeper potential energy, so these states are not emptied with the $zx$ band electrons. Electrons in Nb-Nb bonds would occupy spin-paired bonding states, so the metal-insulator transition need not change significantly the $\mu_{eff}$.

One may wonder why the effects of quantum critical fluctuations, which are usually enhanced as a magnetic phase gives way to a paramagnetic phase, are suppressed in the M phase of $Nb_{12}O_{29}$ under pressure. In all systems where effects of quantum critical fluctuations have been studied, metallic conductivity is found in both the magnetic phase and its adjacent paramagnetic phase. In the M phase of $Nb_{12}O_{29}$, however, $T_N$ does not reduce but the magnetic phase gives
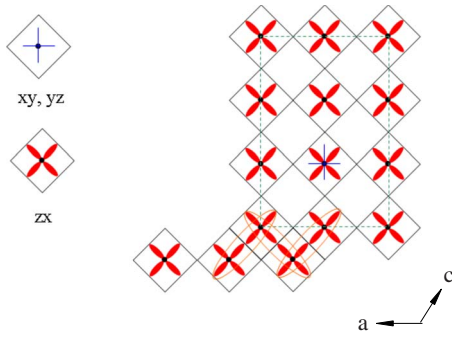
FIG. 10. (Color online) A schematic drawing of partially occupied orbitals in a block of $4 \times 3$ corner-shared $NbO_6$ octahedra. At ambient pressure, one electron spreads in the band state that has primarily $zx$ orbital character; the other electron is localized on a $Nb^{4+}$ site in the center of a block with the occupation of $zx$ and/or $xy \pm iyz$ orbitals. The location of $Nb^{4+}$ has not been determined conclusively from experiments so far. Under high pressure, itinerant electrons likely become trapped on Nb-Nb bonds at interfaces.

way to a paramagnetic insulator under pressure. In this case, itinerant electrons carrying spin fluctuations vanish under pressure. As a matter of fact, the enhancement of $S$ below 70 K remains the same under pressure or even increases slightly as long as a percolation through the metallic phase is still in place. Other evidence of pressure-induced reduction in mobile carries is the absolute value of $S(290$ K$)$, which increases dramatically at $P > 10$ kbar.

### E. Monoclinic phase versus the orthorhombic phase of $Nb_{12}O_{29}$

Even though we have demonstrated the evolution from the M phase to the O phase as a function of annealing temperature, we are still unable to exclude absolutely the M phase in the nominal O phase obtained by firing the sample at 1400 °C. The metallic, antiferromagnetic O phase reported by Cava *et al.*[1] was obtained by annealing the sample at a final temperature 1300 °C. A recent report by Andersen *et al.*[6] has shown that the O phase is paramagnetic down to 4 K. The resistivity study under high pressure by Naka *et al.*[9] was carried out on an O-phase sample that was made in the same way as that reported by Cava *et al.*[1] Although the authors have not provided XRD of the sample they studied, by checking the metallic conductivity and the anomaly of $\rho(T)$ near 12 K under ambient pressure, we believe they were actually working on an M-phase sample. Therefore, a more consistent picture is that the M phase is metallic and becomes antiferromagnetically ordered at about 12 K whereas the O phase is a paramagnetic insulator to the lowest temperature. A very modest pressure, say 10 kbar, would be sufficient to cause a metal-insulator transition within the M phase; this pressure-induced electronic phase transition is reversible as demonstrated by Naka *et al.*[9] in their resistivity measurement under pressure and the thermoelectric power measurement under pressure of this work. We have also shown in Fig. 8 that the M to O phase transition can be realized by applying a hydrostatic pressure $P > 60$ kbar. This pressure-induced phase transition is irreversible as

checked after releasing pressure. It is interesting to compare this high-pressure O phase with that obtained through annealing a sample at ambient pressure. The sample recovered from a DAC after a high-pressure run is too small to measure its transport and magnetic properties. The O_hp sample as confirmed by XRD is a paramagnetic insulator to 5 K. However, the $\mu_{eff}$ from a Curie-Weiss fitting of paramagnetic susceptibility is slightly smaller than that of the O phase reported by Andersen *et al.*[6]

### F. Pressure effect versus the magnetic field effect on the M phase of $Nb_{12}O_{29}$

Since the measurement of resistivity under pressure made by Naka *et al.*[9] has reasonable quality, we have chosen to use their data in our discussion about the M phase instead of repeating the same measurement. The most dramatic pressure effect on $\rho(T)$ occurs at low temperatures; a broad transition from metallic to semiconducting behavior is induced under a modest pressure $P \approx 8.8$ kbar. Figure 6(d) shows a positive MR starting from about 70 K with $H=9$ T and the magnetic field turns the metallic conduction into semiconductive behavior below 10 K. As demonstrated in Figs. 5 and 7, the effects of hydrostatic pressure and magnetic field on the low-temperature enhancement of $S(T)$ are remarkably similar. How can hydrostatic pressure and a magnetic field play the same role on the transport properties in the M phase of $Nb_{12}O_{29}$? Andersen *et al.*[6] have discussed the magnetic to nonmagnetic transition between the M and O phases in the context of the symmetry change in nanometer structural columns that frustrate the spin interactions. Since all discussion here are within the M phase, the symmetry change is not relevant. Within a $4 \times 3$ block, the average bond-length variation in surrounding octahedra is higher than that of the central two octahedra, which signals that electron density is more concentrated in the center of a block. At interfaces between blocks within a (010) layer, the ferroelectric-type displacements in the octahedra crossing an interface are ordered in a way that Nb ions move away from the interface due to Coulombic repulsion. High pressure reduces the ferroelectric displacement so as to decrease the Nb-Nb bond length at interfaces by localizing the $zx$ band electrons into Nb-Nb bonds. Electrons in these metal-metal bonds are likely spin paired so that they contribute no magnetic moment. On the other hand, the exchange oscillation from the RKKY interaction changes sign at the Nb-Nb interface between blocks, which gives AF coupling between the blocks. A sufficiently high magnetic field would break metal-metal bonds with paired electrons so that electrons are forced away from interfaces. In this case, the ferroelectric displacement in the octahedra at interfaces should increase relative to that without a magnetic field and emptying of Nb-Nb bridges between the blocks would break the 2D conduction and also the RKKY coupling between blocks even though $zx$ electrons remain within the blocks. This scenario needs to be confirmed by a structural study under magnetic field. Metallic conductivity in the M phase of $Nb_{12}O_{29}$ appears built on a delicate distribution of electrons between Nb-Nb bonding states at interfaces and the $zx$ band inside the blocks. Both

hydrostatic pressure and a high magnetic field alter the balance so as to destroy the electron itinerancy.

## IV. CONCLUSIONS

The high-temperature magnetic susceptibility had suggested that one of the two $4d$ electrons in a block of $4 \times 3$ corner-shared $NbO_6$ octahedra could be localized, the other itinerant. The structural study in the literature has also indicated the site of $Nb^{4+}$ is located in a block. Results of critical behaviors in this work are consistent with the existence of localized spins that interact with electrons near the Fermi surface responsible for metallic conduction. The quasi-1D crystal structure of the monoclinic $Nb_{12}O_{29}$ phase enhances the thermally driven critical fluctuations near $T_N$. However, the enhancement of thermoelectric power sets in at a temperature well above $T_N$. From the dependences of temperature and magnetic field, the enhancement is likely due to quantum critical fluctuations. Moreover, we have found that a metal-semiconductor transition occurs under $H > 7$ T at low temperatures. The enhanced thermoelectric power and the volume fraction of antiferromagnetic phase in the monoclinic $Nb_{12}O_{29}$ have also been found to be extremely sensitive to hydrostatic pressure; $T_N$ disappears at $P \approx 6$ kbar whereas the enhanced thermoelectric power at low temperature is totally suppressed at $P > 20$ kbar. On the other hand, our high-pressure structural study shows that the monoclinic phase remains stable up to 60 kbar and an irreversible structural transition to the orthorhombic phase, which is a paramagnetic insulator, occurs at $P > 60$ kbar. These observations can be interpreted to be a switching of $4d$ electrons between Nb-Nb bonds at block interface and itinerant-electron states.

*jszhou@mail.utexas.edu

[1] R. J. Cava, B. Batlogg, J. J. Krajewski, P. Gammel, H. F. Poulsen, W. F. Peck, Jr., and W. Rupp, Jr., Nature (London) **350**, 598 (1991).

[2] R. J. Cava, B. Batlogg, J. J. Krajewski, H. F. Poulsen, P. Gammel, W. F. Peck, Jr., and L. W. Rupp, Jr., Phys. Rev. B **44**, 6973 (1991).

[3] P. Mohn, *Magnetism in the Solid State, an Introduction* (Springer-Verlag, Berlin, 2003).

[4] T. Moriya, in *Electron Correlation and Magnetism in Narrow-Band Systems*, edited by T. Moriya (Springer-Verlag, Berlin, 1981), p. 2.

[5] A. Lappas, J. E. L. Waldron, M. A. Green, and K. Prassides, Phys. Rev. B **65**, 134405 (2002).

[6] E. N. Andersen, T. Klimczuk, V. L. Miller, H. W. Zandbergen, and R. J. Cava, Phys. Rev. B **72**, 033413 (2005).

[7] J. E. L. Waldron, M. A. Green, and D. A. Neumann, J. Am. Chem. Soc. **123**, 5833 (2001); J. Phys. Chem. Solids **65**, 79 (2004).

[8] T. McQueen, Q. Xu, E. N. Andersen, H. W. Zandbergen, and R. J. Cava, J. Solid State Chem. **180**, 2864 (2007).

[9] T. Naka, T. Nakane, Y. Furukawa, Y. Takano, T. Adschiri, and A. Matsushita, Physica B **378-380**, 337 (2006).

[10] T. Naka, Mater. Trans. **47**, 501 (2006).

[11] J. E. L. Waldron and M. A. Green, MRS Symposia Proceedings Vol. 658, GG4.5.1 (Materials Research Society, Pittsburgh, 2001).

[12] M. E. Fisher and L. S. Langer, Phys. Rev. Lett. **20**, 665 (1968).

[13] P. P. Craig, W. I. Goldburg, T. A. Kitcens, and J. I. Budnick, Phys. Rev. Lett. **19**, 1334 (1967).

[14] L. W. Shacklette, Phys. Rev. B **9**, 3789 (1974).

[15] F. C. Zumsteg and R. D. Parks, Phys. Rev. Lett. **24**, 520 (1970).

[16] H. Takatsu, H. Yoshizawa, S. Yonezawa, and Y. Maeno, Phys. Rev. B **79**, 104424 (2009).

[17] D. Kim, B. L. Zink, F. Hellman, and J. M. D. Coey, Phys. Rev. B **65**, 214424 (2002).

[18] E. A. Yelland, S. J. C. Yates, O. Taylor, A. Griffiths, S. M. Hayden, and A. Carrington, Phys. Rev. B **72**, 184436 (2005).

[19] S. Sachdev, *Quantum Phase Transitions* (Cambridge University Press, Cambridge, 1999).

[20] G. A. Thomas, K. Levin, and R. D. Parks, Phys. Rev. Lett. **29**, 1321 (1972).

[21] I. Paul and G. Kotliar, Phys. Rev. B **64**, 184414 (2001).

[22] G. Kotliar (private communication).

[23] E. Gratz, H. Nowotny, J. Enser, E. Bauer, and K. Hense, J. Magn. Magn. Mater. **272-276**, E441 (2004).

[24] S. N. Kaul, J. Phys.: Condens. Matter **17**, 5595 (2005).

[25] B. Annie D' Santhoshini and S. N. Kaul, J. Magn. Magn. Mater. **272-276**, 493 (2004).